INTERNATIONAL JOURNAL FOR NUMERICAL METHODS IN FLUIDS, VOL. 8, 1151–1164 (1988)

ONSET OF TRANSITION IN BOUNDARY LAYERS

THORWALD HERBERT

Department of Mechanical Engineering and Department of Aeronautical & Astronautical Engineering, The Ohio State University, Columbus, Ohio 43210, U.S.A.

SUMMARY

Laminar–turbulent transition in boundary layers involves a cascade of weak and strong instabilities. In the model considered here the first instability occurs with respect to two-dimensional TS waves and causes streamwise, nearly periodic concentrations of vorticity. Linear stability analysis of this periodic flow leads to Floquet systems of equations. These systems support different classes of three-dimensional disturbances which may initiate different routes to transition. Numerical solutions by use of accurate spectral methods reveal the spectrum of eigenmodes, growth rates and disturbance velocities. The characteristics of this secondary instability are in good agreement with results of experiments and computer simulations of transition. Non-linear self-interaction of the rapidly growing three-dimensional disturbances can sustain or enhance the vital periodic accumulations of spanwise vorticity once their amplitude exceeds some threshold. This feedback loop is considered to be the key to the transition process. Owing to the broad-band nature of secondary instability, however, the prediction of transition in practice requires additional insight into the 'natural' disturbance background. The sensitivity of the transition process to initial data in a broad band of frequencies and spanwise wave numbers poses new challenges for non-linear theories and numerical simulations.

KEY WORDS Boundary-layer flow Stability Transition

INTRODUCTION

The analysis, prediction and control of transition in boundary layers are of great practical interest. Tremendous efforts have been made with experimental, theoretical and numerical methods to gain insight into the intricate physics of the transition process and to develop a rational theory for predicting transition. Although today's picture of the transition phenomenon is rather detailed, theoretical and computational methods have not yet progressed enough to be incorporated into design-type transition prediction.

For the following we separate the process of transition into four stages: (a) receptivity, (b) primary instability, (c) secondary instability and (d) breakdown.

Design-type transition prediction in a 'natural' environment, e.g. for a cruising airplane, routinely applies the e^n criterion. This criterion rests on the integrated growth rates predicted by the linear stability theory (stage b) but ignores the initial data as well as the non-linear stages of the transition process. The n-factor is correlated with an empirical database of transition measurements.[1] Although this criterion has accrued many merits, it may mislead if used beyond the supporting database. This danger is of some concern for the design of advanced vehicles which are to operate far outside this database.

0271–2091/88/101151–14$07.00

Received 9 September 1987

The 'natural' initial data are a non-uniform spectral mixture of disturbances and are unknown. These initial data are established by the receptivity (stage a) of the boundary layer to sound, turbulence, wall vibrations, roughness, etc. The study of this subject has made some recent progress for special cases[2] but is far from complete. In a similar way progress has been made in analysing the non-linear stages (c an d) for a simplified model of transition. This development will be described in the following.

The experiments of Schubauer and Skramstad[3] and Klebanoff *et al.*[4] initiated a rather detailed phenomenological description of transition in the boundary layer along a flat plate which guided the theoretical efforts for over two decades. The earlier experiments[3] identified the onset of transition with instability to essentially two-dimensional TS waves. Although stability theory predicts a weak preference for two-dimensional waves over oblique waves, the main reasons for the two-dimensionality are the control of the initial disturbances by a vibrating ribbon and the strong receptivity of the boundary layer to vibrations of the leading edge.[5] Besides two-dimensionality of the initial disturbances, the ribbon imposes a preferred frequency and thus selects a single TS mode as the origin of transition. Point sources of disturbances lead to three-dimensional wave packets which can only be reproduced by accounting for a spectrum of TS waves and oblique waves with different frequencies and spanwise wavelengths.[6]

Klebanoff *et al.*[4, 7] observed that the development of the TS wave follows the theoretical predictions only for sufficiently small amplitudes. At amplitudes of about 1%, three-dimensionality develops with a characteristic spanwise periodicity, which in the later experiments was supported by spanwise spacers underneath the ribbon. While the TS wave develops on a slow viscous timescale, three-dimensionality grows rapidly and leads within five TS wavelengths to the appearance of small-scale, high-frequency velocity fluctuations, so called 'spikes'. Breakdown of the laminar flow occurs within one TS wavelength from the onset of spikes.

The origin of three-dimensionality in the experiments has been the target of numerous theories of weakly non-linear wave interactions. In retrospect, only Craik's model of resonant triads[8] turned out to be relevant, after a different type of subharmonic transition was discovered.[9, 10] Herbert and Morkovin[11] suggested that three-dimensional disturbances originate from parametric excitation in the streamwise periodic flow created by the finite-amplitude TS wave. This new concept of secondary instability (stage c) has proved to be very fruitful for studies of various flows and different types of primary disturbances. In the following we briefly summarize the main results for the flat-plate boundary layer and complete the catalogue of three-dimensional disturbances by modes of combination resonance. We report on two ongoing studies to explain and predict the onset of breakdown. Finally we consider the impact of these results on theoretical and computational transition prediction in a 'natural' environment.

LINEAR SECONDARY INSTABILITY

The analysis of secondary instability in boundary layers starts with the observation that finite-amplitude TS waves produce a streamwise, nearly periodic modulation of the basic flow. This modulated flow can be written in the form

$$\mathbf{v}_2(x', y, t) = \mathbf{v}_0(y) + A\mathbf{v}_1(x', y, t), \tag{1}$$

where $\mathbf{v}_0 = \mathbf{v}_0(y)$ represents the boundary layer flow, A the amplitude of the periodic modulation and $\mathbf{v}_1$ a TS wave for given parameters. We denote by x', y, z the streamwise, normal and spanwise direction respectively, and by u, v, w the associated velocity components. We normalize $\mathbf{v}_1$ such

that A is a direct measure for the maximum streamwise RMS fluctuation u'_m. All quantities are non-dimensional using the outer velocity U_∞ and $\delta_r=(\nu L/U_\infty)^{1/2}$ for reference, where L is the distance from the leading edge. Consequently the Reynolds number is $Re=(U_\infty L/\nu)^{1/2}$ and we use the non-dimensional frequency $F=10^6\,\omega c_r/Re$. In a Galilean frame x moving with the TS phase velocity c_r, the basic flow is independent of time and satisfies

$$\mathbf{v}_2(x, y)=\mathbf{v}_2(x+\lambda_x, y), \qquad x=x'-c_r t, \tag{2}$$

where $\lambda_x=2\pi/\alpha$ is the wavelength of the TS wave.

The choice of the basic flow (1) involves three approximations. The first assumption of a locally parallel flow $\mathbf{v}_0$ is well established in the primary stability theory. The second approximation is the locally constant amplitude A of the TS wave. In other words the amplitude A is assumed to vary slowly in comparison with the amplitude B of three-dimensional disturbances. This assumption is justified once three-dimensional disturbances attain sufficient growth rate. The third approximation is the shape assumption, i.e. the neglect of the non-linear distortion of the velocity distribution $\mathbf{v}_1(y)$ at finite amplitude A. This step is justified by the weak non-linear distortion of the u' distribution even at amplitudes of 10% (Hama, personal communication).

The coefficients in the linear stability equations for the basic flow (1) are independent of z and t and periodic in x. According to the theory of differential equations, especially Floquet theory, the equations support three-dimensional disturbances in the form

$$\mathbf{v}_3=\mathrm{e}^{\sigma t}\mathrm{e}^{\gamma x}\mathrm{e}^{\mathrm{i}\beta z}\sum_{m=-\infty}^{\infty}\hat{\mathbf{v}}_m(y)\,\mathrm{e}^{\mathrm{i}2m\hat{\alpha}x}, \tag{3}$$

where $\hat{\alpha}=\pi/\lambda_x$. Owing to the spanwise homogeneity of the basic flow, we consider the spanwise wave number $\beta=2\pi/\lambda_z$ as real, whereas $\sigma=\sigma_r+\mathrm{i}\sigma_i$ and the Floquet exponent $\gamma=\gamma_r+\mathrm{i}\gamma_i$ are in general complex. The Fourier coefficients $\hat{\mathbf{v}}_m(y)$ are governed by an infinite system of ordinary differential equations. Since the physical solution must be real, any complex solution $\mathbf{v}_3$ implies the existence of a complex conjugate solution $\mathbf{v}_3^\dagger$. Consequently the system of equations can be written in a form with real coefficients.

Only two of the four real quantities σ_r, σ_i, γ_r, γ_i, are determined by the eigenvalue problem for $\mathbf{v}_3$. The other two quantities can and must be chosen. Similar ambiguity is associated with the Orr–Sommerfeld problem for TS waves, where the main distinction of different modes is made between temporally and spatially growing waves.[12] For secondary modes temporal growth requires $\gamma_r=0$. The temporal growth rate is given by σ_r, while σ_i can be interpreted as frequency shift with respect to the TS frequency. Modes with $\sigma_i=0$ travel synchronously with the modulated basic flow. Spatial growth in the laboratory frame requires $\sigma_r=\gamma_r c_r$. In this case γ_r is the spatial growth rate, while γ_i is the shift in the streamwise wave number.

Numerical aspects

The derivation of the equations for the Fourier coefficients $\hat{\mathbf{v}}_m$ in equation (3) is straightforward but tedious. Simplifications of the equations arise for the temporal 'tuned' modes with $\gamma=\mathrm{i}k\hat{\alpha}$, k integer.

Primary and secondary stability problems are numerically solved using a spectral collocation method with Chebyshev polynomials. This method converts the ordinary differential equations and boundary conditions into systems of algebraic equations. We prefer the direct treatment of the boundary value problem over shooting methods since we maintain access to spectra of eigenvalues for temporally growing modes. The spectrum is extremely helpful for reliably

identifying the most relevant modes in different regions of the multi-dimensional parameter space and for untangling their analytical connections.

For boundary layers we obtain a finite domain by an algebraic mapping $Y=y_0/(y+y_0)$ that transforms $y=0, \infty$ into $Y=1, 0$ respectively. The parameter y_0 controls the density of collocation points in the neighbourhood of the wall. Only odd Chebyshev polynomials are applied such that the boundary conditions for $y\to\infty$ are automatically satisfied. Typically $J=30$ collocation points are used, and y_0 is chosen to place half of the points within the displacement thickness of the boundary layer. For every (real or complex) function $\hat{v}_m(y)$ in the series (3), $2J+3$ (real or complex) unknowns have to be included in the homogeneous system of algebraic equations. In view of the size of the resulting systems, the truncation of the Fourier series is crucial for the numerical work. Detailed numerical studies[13] have shown that the Fourier series indeed converge rapidly, and the lowest truncation (see below) provides sufficient accuracy for any practical purpose.

The numerical work for tuned modes can be further simplified by exploiting the fact that the physical solution is governed by systems of equations with real coefficients. The solution, however, is only real for real σ. The case of real $\sigma=\sigma_r$ is of particular interest, since synchronization between basic flow and disturbances offers an optimum chance for energy transfer. Since the amplitude A appears linear in the stability equations, real $\sigma(A)$ enables an inverse eigenvalue search for $A(\sigma)$, i.e. the search for the value of the amplitude that produces a given amplification rate. Similar conclusions can be drawn for spatially growing modes.

Concerning the choice between the temporal and spatial growth concept, the situation is analogous to the primary stability analysis. The temporal eigenvalue σ appears linear in the equations. Therefore spectra and single eigenvalues can be obtained by standard procedures of linear algebra. In the spatial formulation the eigenvalue γ appears up to the fourth power. Although methods exist to obtain spectra in this case, the required computations are rather demanding. Therefore we have exploited the fact that neutral behaviour is independent of the growth concept. Parameter combinations for neutral behaviour, $\sigma_r=0$, have been identified using the temporal concept. Starting from these points, the principal eigenvalue can be traced using the spatial concept. The local procedure for spatial eigenvalues γ rests on Newton iteration.

Spatial versus temporal growth

A comparison of the growth characteristics of subharmonic secondary modes for the Blasius boundary layer and for Falkner–Skan profiles using both spatial growth rates and transformed temporal rates[14] verifies that the restriction of Gaster's transformation[12] to small growth rates does not apply to secondary instability. The wave propagation properties of secondary modes are quite different from those of primary modes. For subharmonic modes with $\sigma_i=0$, Bertolotti[15] has shown that c_r is indeed the leading term in the temporal–spatial transformation, with small corrections by dispersive terms. The surprisingly simple relation $\gamma_r\approx\sigma_r/c_r$ between spatial and temporal growth helps to understand the success of temporal computer simulations in reproducing the characteristics of spatially developing transition.

Fundamental and subharmonic modes

While the choice of the growth concept removes the ambiguity in the Orr–Sommerfeld problem, we are still left with one quantity, γ_i, to choose for the modes of secondary instability. This freedom is directly related to the observed non-uniqueness of the three-dimensional stage of transition. For convenience we introduce $\varepsilon=\gamma_i/\alpha$ and distinguish the three cases $\varepsilon=0$, $\varepsilon=1$ and $0<|\varepsilon|<1$. Other values of ε are redundant to within renumbering the Fourier coefficients.

For $\varepsilon=0$ the disturbances (3) can be written in the form

$$\mathbf{v}_f = e^{\sigma t} e^{\gamma_r x} e^{i\beta z} \tilde{\mathbf{v}}_f(x, y), \qquad \tilde{\mathbf{v}}_f = \sum_{m \text{ even}} \hat{\mathbf{v}}_m(y) e^{im\hat{\alpha}x}, \tag{4}$$

where the index f indicates fundamental (or primary) resonance in the Floquet system. Owing to the even multiples m, the streamwise wavelength of these modes coincides with the wavelength λ_x of the basic flow. For the numerical work the lowest truncation of the series retains the Fourier components $\hat{\mathbf{v}}_{-2}$, $\hat{\mathbf{v}}_0$ and $\hat{\mathbf{v}}_2$. Fundamental modes are associated with the peak–valley splitting (K-type) route to transition[16] and with the aligned pattern of Λ vortices in flow visualizations. A computer-generated pattern of particles released from a 'smoke wire' in the critical layer[17] is shown in Figure 1.

Comparison of numerical results for growth rates and disturbance velocities with experiments[4] and computer simulations of transition[18] verifies the theory's capability of predicting the early stage of K-type transition. A similar comparison with more recent measurements[19] shows, however, that the accurate prediction of the streamwise development requires accounting for the non-parallel effect on the TS amplitude A.

For the special case of $\varepsilon=1$ the modes (3) take the form

$$\mathbf{v}_s = e^{\sigma t} e^{\gamma_r x} e^{i\beta z} \tilde{\mathbf{v}}_s(x, y), \qquad \tilde{\mathbf{v}}_s = \sum_{m \text{ odd}} \hat{\mathbf{v}}_m(y) e^{im\hat{\alpha}x}. \tag{5}$$

Owing to the odd values of m, these modes are associated with subharmonic resonance[20, 21] and with the staggered arrangement[22] of Λ vortices as shown in Figure 2. The lowest approximation for subharmonic modes includes only $\hat{\mathbf{v}}_{-1}$ and $\hat{\mathbf{v}}_1$. Numerical results are in excellent agreement with the measurements.[9, 23]

Weak subharmonic instability may occur at arbitrarily small amplitudes owing to resonance of Craik's triad.[8] The conditions for this resonance, however, are strictly satisfied only at a single Reynolds number. For disturbances near resonance conditions to grow from the background to observable levels requires amplification over a range of Reynolds numbers. This requirement can only be satisfied at amplitudes large enough to cause instability in spite of some detuning in frequency and spanwise wave number. The flow visualization of Saric and Thomas[22] at TS

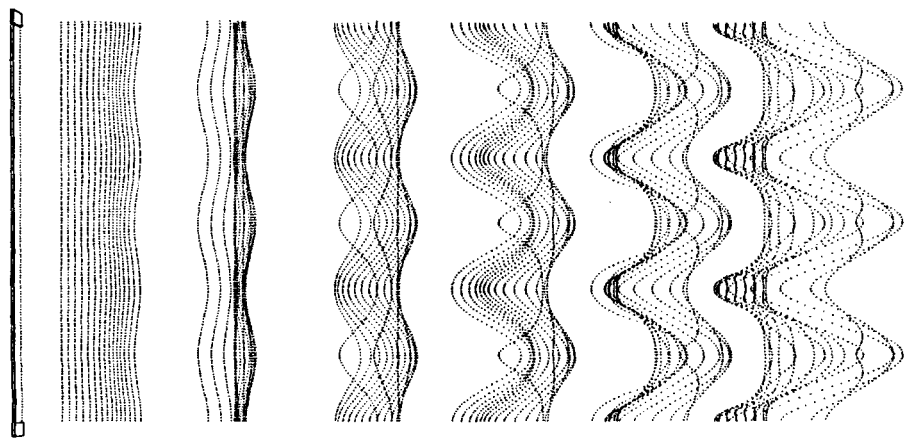

Figure 1. Computer-generated 'aligned' pattern of particles convected in the three-dimensional flow that develops from secondary instability to a fundamental (peak–valley splitting) mode

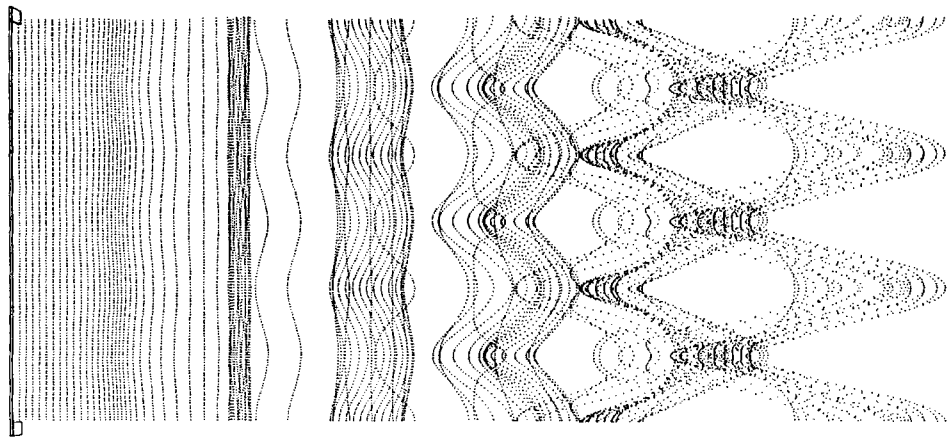

Figure 2. 'Staggered' pattern of particles convected in the three-dimensional flow that develops from secondary instability to a subharmonic mode

amplitudes $A<0{\cdot}3\%$ appears as the 'best fit' to Craik-type resonance. Other components of the background are stable and do not affect the three-dimensional development. There is no guarantee, however, that the subharmonic instability in this case leads to transition. The pattern shown in Reference 22 can be reproduced with our results for linear secondary instability.

For larger amplitudes, $A>0{\cdot}5\%$ say, the principal (most amplified) subharmonic and fundamental modes are phase-locked with the TS wave, $\sigma_i=0$. The growth rates are large in comparison with the maximum growth rate of TS waves. At otherwise fixed parameters the growth rate σ_r (or γ_r) increases with increasing TS amplitude A as well as with increasing Reynolds number Re. Secondary instability occurs in a broad band of spanwise wave numbers β as shown in Figure 3.

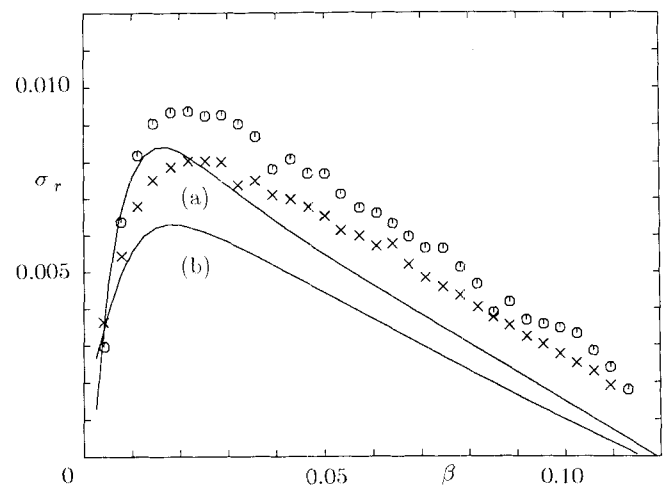

Figure 3. Growth rate of three-dimensional disturbances as a function of the spanwise wave number β for $F=58{\cdot}8$, $Re=950$ and $A=0{\cdot}014$. Theory: (a) subharmonic, (b) peak–valley splitting. Computation:[18] (×) subharmonic, (○) peak–valley splitting

The parameters in Figure 3 are chosen to match the experimental conditions of Klebanoff *et al.*[4] Theoretical and computational results[18] are very similar and both show the stronger amplification of the subharmonic mode. The systematic quantitative differences can be attributed to approximations contained in both theoretical and computational work. The results predict that subharmonic instability should have prevailed in the experiment if the background amplitudes for fundamental and subharmonic modes were equal. The experiments were conducted in a similar region of the stability diagram as later studies[23] on subharmonic resonance. The experimental arrangement, however, especially the spanwise spacers on the plate surface beneath the ribbon, enhanced spanwise periodic mean-flow variations and disturbances of the longitudinal vortex type that directly participate in the resonant mechanism of fundamental instability.

Combination resonance

From a mathematical point of view one expects that neighbouring modes, e.g. with $\varepsilon \approx 0$, will exhibit growth rates in the neighbourhood of those for $\varepsilon = 0$. In physical context the questions arise as to how the growth rate will vary and what the bandwidth (in ε) of this detuned resonance will be. Evidence for the relevance of such detuned modes with $\varepsilon \approx 1$ has been given in experiments[23] which applied two frequencies, the TS frequency F_1 and $F_2 = F_1/2 + \Delta F$, to the vibrating ribbon. Spectra of the velocity field show the response of the boundary layer with two peaks of nearly equal amplitude at the frequencies F_2 and $F_3 = F_1/2 - \Delta F$ such that $F_2 + F_3 = F_1$. The bandwidth of this combination resonance is unexpectedly large.

Detuned modes are contained in the general form (1) of secondary modes for $0 < |\varepsilon| < 1$:

$$\mathbf{v}_d = e^{\sigma t}\, e^{\gamma_r x}\, e^{i\beta z} \sum_{m \text{ even}} \hat{\mathbf{v}}_m(y)\, e^{i(m+\varepsilon)\hat{\alpha}x}. \tag{6}$$

These modes are distinguished from fundamental and subharmonic modes by the intrinsically complex system of equations for the functions $\hat{\mathbf{v}}_m(y)$. The occurrence of real eigenvalues is an unlikely incidence. The loss of synchronization with the basic flow most likely reduces the energy transfer and hence the growth rate as the detuning increases. Moreover, it is obvious that detuned modes lead to combination resonance. The construction of a physical (necessarily real) solution requires two complex conjugate modes with opposite detuning $\pm\varepsilon$. Consequently the real disturbance contains wave numbers $m\hat{\alpha} \pm \gamma_i$ and the sum of such wave number pairs matches the TS wave number. We denote the real combination of two detuned modes as 'combination mode'. Owing to the complex conjugate components, opposite detuning $\pm\gamma_i$ in wave number is conjoint with opposite detuning $\pm\Delta F$ in frequency. The combination modes represent the analytical link between fundamental and subharmonic modes; they are 'something in between'.

Numerical results for the temporal growth of the principal detuned mode[24] are consistent with the observations. Figure 4 shows the growth rate σ_r versus ε at various amplitude levels. At very small amplitudes the fundamental instability is suppressed. A weak near-subharmonic instability persists for the parameters of this figure owing to a detuned triad resonance.[8, 21] Craik's triad resonance was earlier thought to select a subharmonic mode with a characteristic spanwise wavelength. This property is watered down to a weak selectivity with respect to the spanwise wavelength at extremely small amplitudes, with little preference for the tuned subharmonic. As the amplitude increases, the growth rate increases and the instability encompasses the whole range from subharmonic, through detuned, to fundamental modes with comparable growth rates. The stronger subharmonic growth in comparison with fundamental growth has been found for numerous parameter combinations in the medium range of amplitudes and seems to be a generic result consistent with the experience from transition simulations.[18] The higher amplitudes,

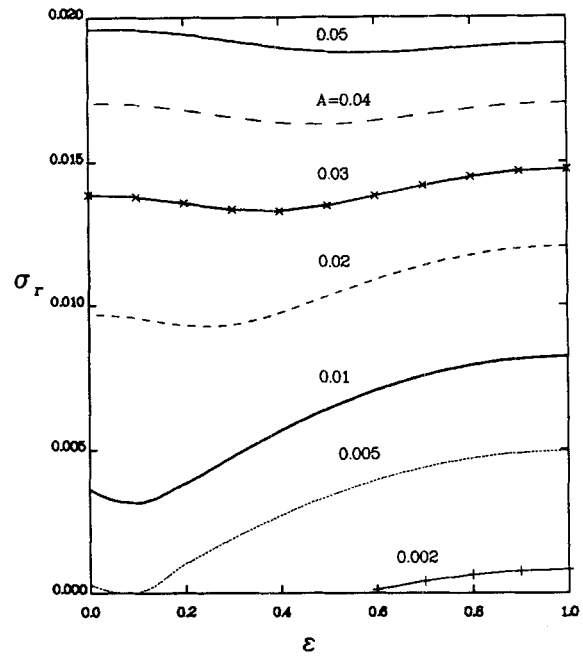

Figure 4. Growth rates of detuned modes as a function of the detuning parameter ε for various amplitudes of the TS wave. $F=124$, $Re=606$, $\alpha=0{\cdot}1017$, $\beta=0{\cdot}2$

$A>1\%$, are not commonly observed in the Blasius boundary layer. From theory and experiment[10] it is known, however, that the wave fetch plays an important role in the development of three-dimensionality from a low-disturbance background. For any mode of instability the amplitude is the result of an initial amplitude combined with the experienced growth. For secondary modes to be observable in a low-disturbance environment requires the conditions for growth to persist for a sufficiently long time or distance. In boundary layers with adverse pressure gradients the stronger TS growth over this distance may lead to the higher amplitude levels used in Figures 4 and 5. For Falkner–Skan profiles it has been found[14] that the main effect of the pressure gradient on secondary instability is the stronger growth of the TS amplitude. At fixed amplitude A the pressure gradient and the associated modification of the basic flow have a rather modest effect on the secondary growth rate σ_r.

The dependency of the growth rate σ_r on the TS amplitude A for $\varepsilon=0$, 0·5, 1·0 is shown in Figure 5 in different form. Whereas the curves are very similar at larger amplitudes, the growth characteristics are different at small TS amplitudes. The threshold amplitudes for the onset of secondary instability are clearly displayed. Figure 5 also shows that $\sigma_r(A)$ behaves differently from the predictions of weakly non-linear theories. According to models of resonant wave interaction,[8] this behaviour should be $\sigma_r \sim A$, while non-resonant models[25] predict $\sigma_r \sim A^2$.

The amplitude growth curves for the TS wave and various associated modes of secondary instability are shown in Figure 6. Frequency F, spanwise wave number β and the TS amplitude level are chosen to mach the experimental conditions of Kachanov and Levchenko.[23] Within the linear framework of the theory, the initial amplitude of the three-dimensional disturbances is arbitrary. Comparison of the curves for different ε gives some appreciation of the selectivity of the secondary instability mechanism. The subharmonic mode grows fastest, but modes in its

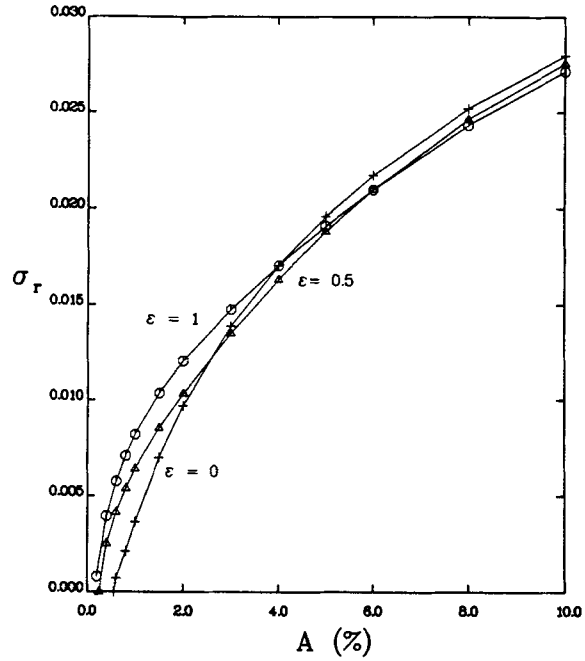

Figure 5. Growth rates of modes with $\varepsilon = 0$, 0·5 and 1·0 as a function of the TS amplitude. $F = 124$, $Re = 606$, $\hat{\alpha} = 0{\cdot}1017$, $\beta = 0{\cdot}2$

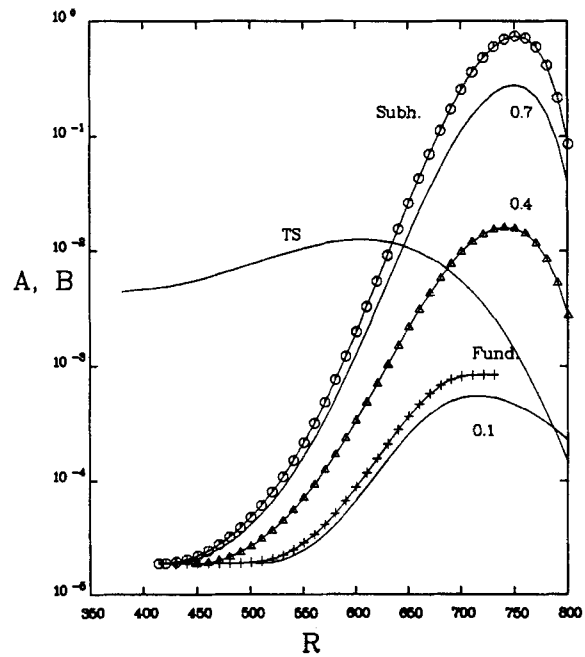

Figure 6. Streamwise variation of the TS amplitude A and the amplitude B of secondary modes with different detuning

neighbourhood reach considerable amplitude. The overall growth of the fundamental mode is rather modest.

Whereas the TS wave decays downstream of branch II ($Re \approx 606$) of the neutral curve, the three-dimensional modes continue to grow. Since σ_r grows with Re at constant A, the maximum growth occurs downstream of branch II.[21] After this point σ_r decreases and the three-dimensional modes reach a maximum amplitude further downstream of branch II where $\sigma_r = 0$. Subsequently the three-dimensional modes decay, since the vitally important parametric excitation fades away. This general picture of the growth curve for secondary modes is consistent with observations at low TS amplitude levels in a low-disturbance environment.[22, 23] It is clear, however, that this picture will require modification once the non-linear self- and cross-interaction of secondary modes and TS wave cannot be neglected, as will be discussed below.

The visualization of a combination mode is shown in Figure 7 for $\varepsilon = \pm 0{\cdot}4$. For this strong detuning the streamwise changing arrangement—sometimes staggered, sometimes aligned—of the leading and trailing parts of particle lines is clearly discernible. At smaller detuning these changes require larger distance and may not be visible in (less accurate) laboratory visualizations. Still pictures taken at different times may show different arrangements of Λ vortices. However, the different modes can be clearly distinguished in spectra of the fluctuations.

NON-LINEAR ASPECTS

The Floquet analysis of linear secondary instability predicts the characteristics of the early three-dimensional stages of transition. The later stages involve a strong interaction of three-dimensional disturbances with the mean flow and the TS wave. The need to account for non-linear effects is obvious in view of the strong growth of secondary modes and is clearly shown by experimental and computational results.

At low levels of the TS amplitude secondary disturbances may grow but ultimately decay with the TS wave as shown in Figure 6. At higher TS amplitude the stronger growth from the same initial level can lead to amplitudes of the three-dimensional modes large enough to affect the two-dimensional wave development and to prevent the decay of the two-dimensional component. In this way primary and secondary disturbances team up to generate a rapid evolution toward breakdown.

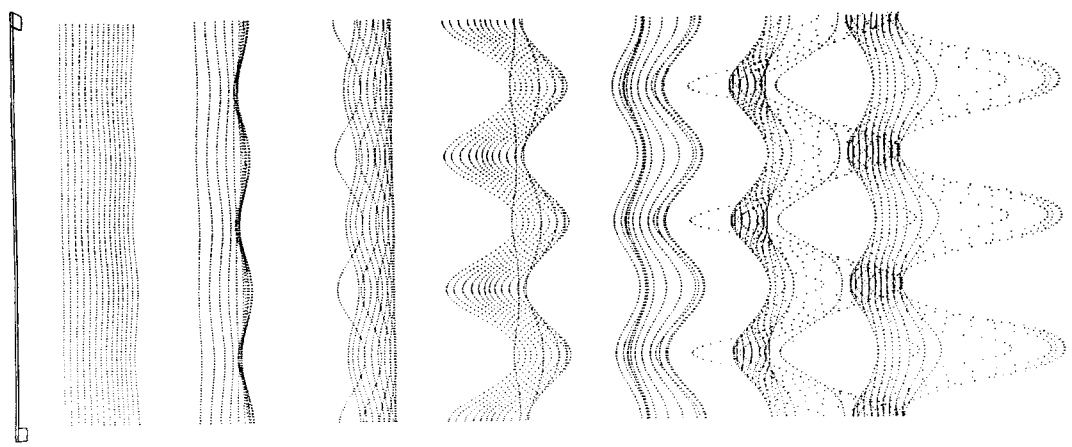

Figure 7. Pattern of particles convected in the three-dimensional flow that develops from secondary instability to a combination mode with $\varepsilon = \pm 0{\cdot}4$. Note the alternating appearance of aligned and staggered arrangement of the structures

As a first step toward exploring the non-linear interaction between the components of the flow field, we have analysed the vorticity field and its relation to the energy transfer between mean flow $\mathbf{v}_0$, two-dimensional wave $A\mathbf{v}_1$ and three-dimensional disturbances $B\mathbf{v}_3$. The origin of secondary instability can be clearly tracked to the streamwise periodic concentrations of the spanwise vorticity created by the primary wave. The TS wave plays only a catalytic role in mediating the transfer of energy from the mean flow into three-dimensional disturbances.[26] Secondary instability reflects the dynamics of disbributed vortices in a shear flow.

While similar results for the boundary layer are forthcoming, we use some key results from a study of plane Poiseuille flow.[27, 28] For sufficiently large TS amplitudes this study shows that the energy transfer is highly localized. For unstable TS waves the distribution of the power in the x, y plane shows shallow extrema near the critical layer, spreads far away from the wall and is periodic in x with wavelength $\lambda_x/2$. Averaging in the streamwise direction provides a sharp peak at the critical layer. Integration normal to the wall yields the small positive growth rate (multiplied by twice the energy of the TS wave). For fundamental and subharmonic secondary modes the picture changes drastically. The spanwise-averaged power has sharp oval peaks near the centre of the cat's eyes, a clear indicator of the close association between vorticity distribution and secondary instability. A similar concentration of the streamwise-averaged power can be seen in the y, z plane normal to the mean flow direction. A more detailed scan reveals that the energy transfer into secondary modes is confined to shallow ellipsoids centred above the critical layer and at the positions where the deflection of the distributed spanwise vortices is strongest.

The observation of this highly localized energy transfer stimulates some speculation. The tie to the critical layer stems from creating the array of distributed vortices by a TS wave. Such an array created in another way at a different distance from the wall and convected with the local mean velocity will behave similarly to within changes in shear and viscous effects. Because of the broad-band nature of the secondary instability, spanwise periodicity of the three-dimensional disturbance will not be necessary. A single twist or kink may be enough to create a patch of Λ vortices. Small curvature, small variation in strength and finite spanwise extent of the vortices like the crests of a wave packet will barely cause dramatic changes. We therefore expect secondary instability to occur in the 'natural' situation, which is characterized by a spotty appearance of wave packets. The spanwise and streamwise periodicity is essential for the pattern formation and distinction of various modes. The streamwise wavelength determines the spanwise scale of the pattern. However, the pattern is not vital to transition. A single vortex convected with the local mean velocity and exposed to a single kink should reveal the elemental dynamics of the early stages of transition. Stuart[29] studied periodic disturbances of a single vortex and found scales similar to those in the experiments.[4] Further study of this phenomenon might reveal the secret of 'bypasses' of the stages of instability in noisy environments.

While the localized energy transfer permits abstraction from the doubly periodic model of secondary instability, the attempt to identify criteria for the onset of self-sustained growth of three-dimensional disturbances is closely tied to this model.

At comparable amplitudes of two-dimensional and three-dimensional disturbances in the range of 1%, the total energy transfer from the mean flow into the secondary disturbances exceeds the maximum viscous transfer into the TS wave by more than an order of magnitude. Typically only a third of this energy is dissipated, but not all the remainder is converted into growth of the three-dimensional component. About a tenth of the energy received is transferred into the two-dimensional field. This observation gives a first lead toward the feedback loop of self-sustained growth of three-dimensional disturbances. Our conclusions from the analysis of the global energy balance is illustrated in Figure 8.

(1) For unstable TS waves the transfer of energy from the mean flow to the two-dimensional

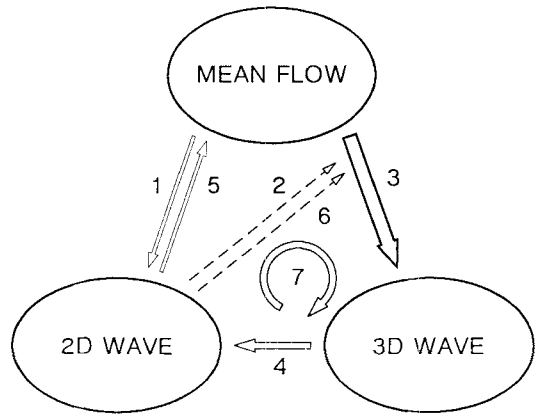

Figure 8. Illustration of the energy transfer between mean flow, two-dimensional wave and three-dimensional disturbances. The numbers refer to the text

wave is weak owing to the viscous mechanism; a considerable part of the energy gained is dissipated. (2) At sufficiently large amplitude A the two-dimensional wave leads to parametric excitation of three-dimensional modes. (3) This excitation causes strong energy transfer from the mean flow into the three-dimensional wave. One part of this energy is dissipated, a second part increases the amplitude B of the three-dimensional wave. Steps 2 and 3 agree with the results of transition simulations[26] for the instability of large-amplitude periodic motions. (4) A third part of the energy gained is transferred into the two-dimensional wave. This transfer draws a minor amount off the three-dimensional growth but boosts the modest energy budget of the two-dimensional wave; the gain in growth rate is proportional to B^2/A. (5) Once B has attained a sufficiently large value, the energy of the two-dimensional wave can increase even if the TS mechanism fails to support this growth. This conclusion is consistent with computational results.[18] (6) Provided the gain in energy maintains the vital catalytic effect of the two-dimensional field, it enhances the growth of B. (7) Parametric excitation of three-dimensional disturbances by the two-dimensional field they create establishes a positive feedback loop and leads to self-sustained simultaneous growth of two-dimensional and three-dimensional waves. The existence of such a loop is supported by experience, experiment and computation.

Threshold conditions for self-sustained growth

The energy analysis involves approximations and neglects non-linear effects such as the distortion of the velocity profiles and the generation of harmonics. A more appropriate model of the non-linear interaction[30] is based on the momentum equations and on perturbation expansions about the periodic basic flow of a given amplitude A^*. The model consists of two modes of secondary instability, the first of which is two-dimensional. This mode describes the instability of the basic flow in a strictly two-dimensional framework. The second mode is either a subharmonic or fundamental mode of three-dimensional instability. Similarly to the energy analysis, the expansion yields up to second order the amplitude equations

$$\frac{\mathrm{d}\hat{A}}{\mathrm{d}t}=a_0\hat{A}+a_1\hat{A}^2+a_2B^2, \qquad \frac{\mathrm{d}B}{\mathrm{d}t}=b_0B+b_1\hat{A}B, \tag{7}$$

where $\hat{A}=A-A^*$ and a_0 and b_0 are the linear growth rates of the secondary modes. The parametric effect of A on the three-dimensional growth rate is represented by $b_1>0$. The unusual self-interaction of the two-dimensional mode at second order is caused by the periodic character of the basic flow, and a_1 is of minor importance. Of prime interest is the coefficient a_2 which incorporates the effect of the three-dimensional disturbance on the two-dimensional mode. In accordance with the energy analysis, this effect is proportional to B^2, and a_2 is expected to be positive and large in comparison with $|a_1|$ whenever A^* is sufficiently large. For $a_0\hat{A}+a\hat{A}^2>0$ the two-dimensional mode will always grow and this growth will be enhanced if $a_2>0$. For $a_0\hat{A}+a_1\hat{A}^2\leqslant 0$ the two-dimensional wave will grow only if B exceeds the threshold value B_t, where $B_t^2=-(a_0\hat{A}+a_1\hat{A}^2)/a_2$. The numerical results of the rather intricate analysis are in the final stages of verification.

DISCUSSION

The amplification of initial disturbances in a broad band of frequencies and spanwise wave numbers shows that our present picture of transition is strongly biased by the few experimental descriptions of the phenomena. The model of ribbon-induced transition and, to an even greater extent, the temporal transition simulations in a spatially periodic domain provide insight into highly idealized situations. Although numerical simulations could predict the onset of breakdown without resolving the small scales of the spike stage, the incorporation of spanwise and streamwise selection mechanisms pioneered by Spalart and Yang[18] exceeds current computer capacity. Whereas the difference between temporal and spatial growth characteristics appears less dramatic than thought earlier, the incorporation of realistic boundary layers into the temporal simulations is difficult. The specification of transparent downstream boundary conditions for spatial simulations, on the other hand, is still an unsolved problem. For more theoretical studies we can currently identify three key areas of future research. The first area aims at increasing insight into the spectral properties of noise in 'natural' environments, uncontrolled but biased test facilities and controlled experiments. Deeper understanding of receptivity is an integral part of this issue. The second area is the incorporation of streamwise variations of boundary layer profile, primary instability modes and secondary instability modes into the analysis. Fortunately the effect of non-linearity is negligible for most of the early stages. Finally the tools have to be developed to deal with the non-linear evolution of single modes and with the wealth of non-linear wave interactions in the late stages of transition.

ACKNOWLEDGEMENTS

I am grateful to German R. Santos, Fabio P. Bertolotti, Joseph W. Croswell and Jeffrey D. Crouch, who contributed valuable ideas and results. This work is supported by the Air Force Office of Scientific Research under Contract F49620-87-K-0005.

REFERENCES

1. E. Reshotko, 'Boundary-layer stability and transition', *Ann. Rev. Fluid Mech.*, **8**, 311–349 (1976).
2. E. Reshotko, 'Stability and transition, how much do we know?', in J. P. Lamb (ed.), *Proc. 10th U. S. Nat. Congr. on Applied Mechanics*, Austin, Texas, 1986, ASME, 1987, pp. 421–434.
3. G. B. Schubauer and H. K. Skramstad, 'Laminar boundary-layer oscilllations and transition on a flat plate', *J. Res. N. B. S.*, **38**, 251–292 (1947) (reprint of *NACA Adv. Conf. Rep.*, 1943).
4. P. S. Klebanoff, K. D. Tidstrom and L. M. Sargent, 'The three-dimensional nature of boundary-layer instability', *J. Fluid Mech.*, **12**, 1–34 (1962).
5. M. Nishioka and M. V. Morkovin, 'Boundary-layer receptivity to unsteady pressure gradients: experiments and overview', *J. Fluid Mech.*, **171**, 219–261 (1986).

6. M. Gaster, 'A theoretical model of a wave packet in the boundary layer on a flat plate', *Proc. Roy. Soc. Lond. A*, **347,** 271–289 (1975).
7. P. S. Klebanoff and K. D. Tidstrom, 'Evaluation of amplified waves leading to transition in a boundary layer with zero pressure gradient', *NASA TN D-195*, 1959.
8. A. D. D. Craik, 'Nonlinear resonant instability in boundary layers', *J. Fluid Mech.*, **50,** 393–413 (1971).
9. Yu. S. Kachanov and V. Ya. Levchenko, 'Resonant interactions of disturbances in transition to turbulence in a boundary layer', *Preprint No. 10–82*, ITAM, USSR Academy of Sciences, Novosibirsk, 1982 (in Russian).
10. A. S. W. Thomas, 'Experiments on secondary instabilities in boundary layers', in J. P. Lamb (ed.), *Proc. 10th U. S. Nat. Congr. on Applied Mechanics*, Austin, Texas, 1986, ASME, 1987, pp. 436–444.
11. Th. Herbert and M. V. Morkovin, 'Dialogue on bridging some gaps in stability and transition research', in R. Eppler and H. Fasel (eds), *Laminar–Turbulent Transition*, Springer-Verlag, 1980, pp. 47–72.
12. M. Gaster, 'A note on the relation between temporally-increasing and spatially-increasing disturbances in hydrodynamic stability', *J. Fluid Mech.*, **14,** 222–224 (1962).
13. F. P. Bertolotti, G. R. Santos and Th. Herbert, 'Early stages of boundary-layer transition—an animated theory', *16 mm movie*, VPI & SU, 1986.
14. Th. Herbert and F. P. Bertolotti, 'Effect of pressure gradients on the growth of subharmonic disturbances in boundary layers', in T. J. Mueller (ed.), *Proc. Conf. on Low Reynolds Number Airfoil Aerodynamics*, University of Notre Dame, 1985.
15. F. P. Bertolotti, 'Temporal and spatial growth of subharmonic disturbances in Falkner–Skan flows', *M.S. Thesis*, VPI & SU, 1985.
16. Th. Herbert, 'Three-dimensional phenomena in the transitional flat-plate boundary layer', *AIAA Paper No. 85–0489*, 1985.
17. F. P. Bertolotti and Th. Herbert, 'A study on visualizations of boundary-layer transition', *Exp. Fluids*, (1988) (in preparation).
18. P. R. Spalart and K. S. Yang, 'Numerical simulation of boundary layers: Part 2. Ribbon-induced transition in Blasius flow', *NASA Technical Memorandum 88221*, 1986, pp. 1–24.
19. K. C. Cornelius, 'Three dimensional wave development during boundary layer transition', *Lockheed Georgia Research Report LG85RR0004*, 1985.
20. Th. Herbert, 'Subharmonic three-dimensional disturbances in unstable shear flows', *AIAA Paper No. 83-1759*, 1983.
21. Th. Herbert, 'Analysis of the subharmonic route to transition in boundary layers', *AIAA Paper No. 84-0009*, 1984.
22. W. S. Saric and A. S. W. Thomas, 'Experiments on the subharmonic route to turbulence in boundary layers', in T. Tatsumi (ed.), *Turbulence and Chaotic Phenomena in Fluids*, North-Holland, 1984, pp. 117–122.
23. Yu. S. Kachanov and V. Ya. Lavchenko, 'The resonant interaction of disturbances at laminar–turbulent transition in a boundary layer', *J. Fluid Mech.*, **138,** 209–247 (1984).
24. G. R. Santos and Th. Herbert, 'Combination resonance in boundary layers', *Bull. Am. Phys. Soc.*, **31,** 1718 (1986).
25. D. J. Benney and C. C. Lin, 'On the secondary motion induced by oscillations in a shear flow', *Phys. Fluids*, **3,** 656–657 (1960).
26. S. A. Orszag and A. T. Patera, 'Secondary instability of wall-bounded shear flows', *J. Fluid Mech.*, **128,** 347–385 (1983).
27. J. W. Croswell, 'On the energetics of primary and secondary instabilities in plane Poiseuille flow', *M. S. Thesis*, VPI & SU, 1985.
28. Th. Herbert, 'Vortical mechanisms in shear flow transition', in U. Schumann and R. Friedrich (eds), *Direct and Large Eddy Simulation of Turbulence*, Vieweg-Verlag, 1986, pp. 19–36.
29. J. T. Stuart, 'The production of intense shear layers by vortex stretching and convection', *AGARD Report 514*, 1985.
30. J. D. Crouch and Th. Herbert, 'Perturbation analysis of nonlinear secondary instability in boundary layers', *Bull. Am. Phys. Soc.*, **31,** 1718 (1986).